Table S9. Results of serum biochemical tests following chronic toxicity tests in rabbits

Test	Date	Control	A549	AdE3-*IAI.3B*	Carrier cells (dose) low	moderate	high
ALT	Pre	57±23	58±14	51±14	58±19	63±24	58±22
(U/L)	Week 2	59±18	73±39	55±11	43±8*	53±6	52±21
	Week 4	96±41	67±20	67±17	56±18*	55±12*	63±14*
	Week 8	113±27	80±22	79±25	67±39	114±11	75±27
AST	Pre	43±10	42±13	43±8	48±14	45±6	51±21
(U/L)	Week 2	41±10	44±10	38±10	43±10	48±13	44±19
	Week 4	64±30	43±19	46±17	50±17	41±9*	42±4
	Week 8	66±16	53±7	40±5*	55±34	90±29	41±19
ALP	Pre	97±52	89±31	77±26	112±21	95±45	92±34
(U/L)	Week 2	75±38	62±21	68±24	51±16	46±19*	38±16*
	Week 4	80±19	65±20	80±21	52±13*	51±17*	56±19*
	Week 8	112±26	105±24	103±13	98±16	129±44	99±18
γ -GTP	Pre	5.0±1.5	5.7±2.8	4.2±2.8	6.7±3.2	5.6±2.9	5.4±2.7
(U/L)	Week 2	5.2±1.9	6.4±4.5	5.2±2.1	4.2±2.0	4.8±2.1	5.0±3.8
	Week 4	7.5±2.9	5.9±5.3	5.8±1.7	3.4±2.0*	4.2±2.0*	4.4±2.9*
	Week 8	8.0±1.4	8.0±5.2	8.5±2.4	7.0±1.4	8.5±1.0*	5.7±1.5
TP	Pre	62.9±6.5	62.7±6.7	60.9±8.5	68.9±9.3	59.4±11.8	62.3±34
(g/L)	Week 2	65.9±3.9	66.1±6.5	65.8±7.8	67.3±5.5	66.8±4.5	65.1±8.2
	Week 4	67.4±4.0	72.2±5.9	69.0±5.7	75.3±4.7*	74.4±5.4*	84.5±5.4*
	Week 8	65.3±7.2	67.6±1.7	65.0±2.3	68.3±3.7	68.3±3.4	69.8±2.4
ALB	Pre	19.4±3.6	19.8±3.3	18.5±4.4	22.3±2.7	19.4±3.9	19.7±3.6
(g/L)	Week 2	21.7±2.6	20.7±3.7	20.8±2.8	19.4±2.1*	18.6±1.6*	16.8±2.5*
	Week 4	27.7±1.8	26.0±2.9	26.8±1.6	24.8±1.0*	23.3±1.9*	24.3±1.5*
	Week 8	27.3±2.2	27.4±1.0	26.2±0.5	26.4±2.8	26.6±0.6	26.7±0.8

ALT, alanine aminotransferase; AST, aspartate aminotransferase; ALP, alkaline phosphatase; γ-GTP, gamma-glutamyl transpeptidase; TP, total protein; ALB, albumin; Carrier cells, AdE3-*IAI.3B*-infected A549 cells; *, $P < 0.05$.

Table S10. Results of serum biochemical tests following chronic toxicity tests in rabbits

Test	Date	Control	A549	AdE3-*IAI.3B*	Carrier cells (dose) low	moderate	high
TCHO	Pre	1.0±0.3	1.2±0.4	1.5±0.6*	1.3±0.4	1.3±0.4	1.2±0.5
(mmol/L)	Week 2	1.3±0.8	1.5±0.5	1.3±0.3	1.4±0.5	1.8±1.2	2.7±1.6*
	Week 4	1.1±0.2	1.3±0.4	1.4±0.3*	1.8±0.6*	2.3±1.3	2.4±1.1
	Week 8	1.4±0.4	1.7±0.1	2.3±0.6*	1.8±0.3	2.2±0.8	2.1±0.6*
TG	Pre	1.3±0.5	1.2±0.7	2.1±1.3	1.2±0.7	1.5±1.3	1.5±1.3
(mmol/L)	Week 2	1.7±0.6	2.0±0.7	1.9±0.7	1.9±0.5	1.9±0.7	3.4±1.9*
	Week 4	1.2±0.5	1.3±0.4	1.2±0.3	1.7±0.6	1.6±0.5	2.2±0.7*
	Week 8	1.5±0.3	1.0±0.4	1.4±0.6	1.1±0.4	1.3±0.1	1.4±0.4
BUN	Pre	8.3±1.2	8.3±2.0	7.9±1.7	7.2±2.4	8.8±1.8	8.4±2.1
(mmol/L)	Week 2	6.2±2.4	7.1±1.2	6.0±1.3	5.8±1.1	6.2±1.1	7.1±4.1
	Week 4	9.6±3.0	9.2±2.0	8.9±2.7	8.8±1.6	8.0±1.8	8.8±3.1
	Week 8	7.1±1.0	6.3±0.2	6.5±0.6	6.9±0.4	6.7±0.8	6.9±1.2
Creat	Pre	107±11	102±11	106±18	113±16	111±18	109±15
(μmol/L)	Week 2	93±10	89±12	98±10	95±18	91±9	70±27*
	Week 4	125±18	110±9	122±15	113±16	113±14	109±16
	Week 8	124±11	131±15	137±6	138±12	133±6	134±18
CK	Pre	2275±1037	2432±1246	2381±865	2334±899	2803±1347	2390±1223
(U/L)	Week 2	2701±1512	2826±1321	2100±816	3450±903	3355±1221	3262±1638
	Week 4	1582±508	1260±534	1574±700	2331±882*	1985±858*	1639±1323
	Week 8	922±154	1191±163	1357±511	1091±536	1591±499	1019±150
GLU	Pre	5.8±1.1	6.3±1.3	5.2±1.6	5.8±1.5	5.9±1.2	6.2±1.7
(μmol/L)	Week 2	5.0±1.0	5.4±1.2	5.2±0.7	5.1±1.1	5.3±1.1	5.7±1.3
	Week 4	5.9±0.9	5.9±1.0	5.7±1.5	7.3±2.5	6.1±1.9	6.3±1.3
	Week 8	6.2±0.7	5.9±0.5	6.0±0.2	5.7±0.8	5.9±0.9	6.2±1.2

TCHO, total cholesterol; TG, triglyceride; BUN, blood urea nitrogen; Creat, creatinine; CK, creatine kinase; GLU, glucose; Carrier cells, AdE3-*IAI.3B*-infected A549 cells; *, $P < 0.05$.

Periostin accelerates human malignant melanoma progression by modifying the melanoma microenvironment

Yorihisa Kotobuki[1,2,a], Lingli Yang[1,a], Satoshi Serada[2], Atsushi Tanemura[1], Fei Yang[1], Shintaro Nomura[3], Akira Kudo[4], Kenji Izuhara[5], Hiroyuki Murota[1], Minoru Fujimoto[2], Ichiro Katayama[1] and Tetsuji Naka[2]

1 Department of Dermatology, Osaka University Graduate School of Medicine, Suita, Japan 2 Laboratory for Immune Signal, National Institute of Biomedical Innovation, Ibaraki, Japan 3 Department of Animal Bioscience, Nagahama Institute of Bio-Science and Technology, Nagahama, Japan 4 Department of Biological Information, Tokyo Institute of Technology, Yokohama, Japan 5 Division of Medical Biochemistry, Department of Biomolecular Sciences, Saga Medical School, Saga, Japan

CORRESPONDENCE Atsushi Tanemura, *e-mail: tanemura@derma.med.osaka-u.ac.jp*

[a]These two authors contributed equally to this work.

KEYWORDS periostin/malignant melanoma/tumor microenvironment

PUBLICATION DATA Received 29 May 2013, revised and accepted for publication 24 March 2014, published online 26 March 2014

doi: 10.1111/pcmr.12245

Summary

Given no reliable therapy for advanced malignant melanoma, it is important to elucidate the molecular mechanisms underlying the disease progression. Using a quantitative proteomics approach, the 'isobaric tags for relative and absolute quantitation (iTRAQ)' method, we identified that the extracellular matrix protein, periostin (POSTN), was highly expressed in invasive melanoma compared with normal skin. An immunohistochemical analysis showed that POSTN was expressed in all invasive melanoma (n = 20) and metastatic lymph node (n = 5) tissue samples, notably restricted in their stroma. In terms of the intercellular regulation of POSTN, we found that there was upregulation of POSTN when melanoma cells and normal human dermal fibroblasts (NHDFs) were cocultured, with restricted expression of TGF-β1 and TGF-β3. In a functional analyses, recombinant and NHDF-derived POSTN significantly accelerated melanoma cell proliferation via the integrin/mitogen-activated protein kinase (MAPK) signaling pathway in vitro. The size of implanted melanoma tumors was significantly suppressed in *POSTN/Rag2* double knockout mice compared with *Rag2* knock-out mice. These results indicate that NHDF-derived POSTN accelerates melanoma progression and might be a promising therapeutic target for malignant melanoma.

Significance

In this study, we found an extracellular matrix protein, periostin (POSTN), increased in invasive melanoma compared with radial growth melanoma a quantitative proteomics approach, the 'isobaric tags for relative and absolute quantitation (iTRAQ)' method. POSTN was exclusively expressed in the tumor-associated stromal tissue not in the tumor cells, suggesting the paracrine effect of POSTN to melanoma cells aggressiveness. As expected, secreted POSTN could augment cell proliferation in melanoma cell lines in vitro. Moreover, we generated of *postn* and *rag2* double knockout mice and showed significant inhibition of human melanoma growth in those *KO* mice in vivo. This study could give us the cue of therapeutic effect on melanoma growth by an agent controlling tumor microenvironment induced by POSTN.

Introduction

Malignant melanoma is one of the most aggressive malignancies due to its strong capacity to grow, invade and metastasize, and therefore, it is of high priority to identify novel therapeutic targets and treatment options for this cancer.

Periostin (POSTN), first described in 1993 in mouse osteoblasts as osteoblast-specific factor 2 (OSF-2), is a secreted matrix N-glycoprotein of 93 kDa (Takeshita et al., 1993). The N-terminal region contains four fasciclin-like domains as well as several glycosylation sites. The protein originally was identified in MC3T3-E1 osteoblast-like cells, where it promotes integrin-dependent cell adhesion and motility. It shares homology with the insect cell adhesion molecule fasciclin I, with human β IgH3, and is induced by transforming growth factor-β (TGF-β) (Horiuchi et al., 1999), bone morphogenic protein-2 (Inai et al., 2008), IL-4, IL-13 (Takayama et al., 2006), and PDGF-bb (Li et al., 2006). As a ligand to alpha(V)beta(3) and alpha(V)beta(5) integrins, POSTN appears to activate the Akt/PKB (protein kinase B) pathway, which is known to facilitate cell survival and tumorigenesis (Bao et al., 2004; Gillan et al., 2002; Yan and Shao, 2006).

POSTN promotes the epithelial–mesenchymal transition (EMT), cancer cell growth, angiogenesis, invasiveness, and metastasis in several cancers (Bao et al., 2004; Baril et al., 2007; Erkan et al., 2007; Gillan et al., 2002; Kudo et al., 2006; Li et al., 2002; Puppin et al., 2008; Riener et al., 2010; Sasaki et al., 2001, 2002, 2003; Shao et al., 2004; Soltermann et al., 2008a,b; Tilman et al., 2007; Tischler et al., 2010). Although it was also reported that melanomas expressed POSTN (Tilman et al., 2007), the precise roles and the source of POSTN in malignant melanoma are still unclear.

We investigated the functional role of POSTN during melanoma tumor progression in vitro *and* in vivo. Moreover, we herein demonstrate that stromal cells, normal human dermal fibroblasts (NHDFs), were important sources of POSTN in cutaneous malignant melanoma and that NHDFs promote tumor growth and progression and modulate the tumor microenvironment by secreting POSTN in cutaneous malignant melanoma.

Results

Protein expression profiles in melanoma and normal skin

To identify the proteins associated with the progression of melanoma, we performed comparative protein expression profiling between in situ melanoma tissues and matched normal skin tissue, or between invasive melanoma tissue and matched normal skin tissues. We identified a total of 1062 proteins, and 1036 proteins were quantitatively analyzed by the iTRAQ 4-plex technology using a nano LC-MS/MS analysis. The complete list of all proteins identified is shown in Table S1. Among the identified proteins present at different levels in the invasive melanoma lesions compared with matched normal skin, 30 proteins were found to have increased more than 15-fold, while 67 proteins decreased to <0.25-fold (Table S1). As expected, S100, a protein previously known to be overexpressed in melanoma, was identified as one of the overexpressed proteins. Interestingly, POSTN was found to have a 25.703-fold higher expression in invasive tumor tissue compared with matched normal skin and showed a 4.434-fold higher expression in in situ tissue compared with matched normal skin (Table S1).

Expression of POSTN in melanomas

To confirm the altered expression of POSTN in invasive melanoma, we performed a Western blot analysis using proteins extracted from the same samples. As shown in Figure 1, POSTN was highly expressed in invasive melanoma tissue and slightly expressed in in situ tissue, although POSTN was faint in normal skin tissue (Figure 1A).

We thereafter preformed an immunohistochemical analysis of 20 invasive melanoma tissues and five metastatic lymph nodes. The expression of POSTN was observed in all invasive melanoma tissue samples and metastatic lymph nodes (Figure 1B). POSTN was localized in the stroma of the invasive melanoma, with a mesh-like structure (Figure 1C). Together, these data demonstrate that POSTN was overexpressed in invasive melanoma at the protein level; this was consistent with the results of our iTRAQ analysis.

POSTN is produced by NHDF instead of melanoma cells

We also analyzed the expression of POSTN in the cell lysates from three melanoma cell lines (MeWo, G-361, and VMRC-MELG) and melanocytes by Western blot analysis; however, the expression of POSTN was not observed in these cells (Figure 2A). Because POSTN was expressed in melanoma tissue samples, but not in melanoma cell lines, we hypothesized that an interaction between melanoma cells and NHDFs was required for the optimum expression of POSTN. First, we cocultured NHDFs with the MeWo, G-361, and VMRC-MELG cell lines and performed RT-PCR and a Western blot analysis. An overexpression of POSTN mRNA was only observed in the cocultured cell lysates (Figure 2B), and POSTN protein was detected in the cocultured supernatant in a time-dependent manner (Figure 2C).

To identify the source of POSTN, we cocultured NHDFs with CFSE-labeled MeWo cells for 48 h, and sorted these cells into NHDF and MeWo populations. The expression of POSTN mRNA measured by RT-PCR showed the source of the POSTN to be the NHDFs, not the MeWo cells (Figure 2D).

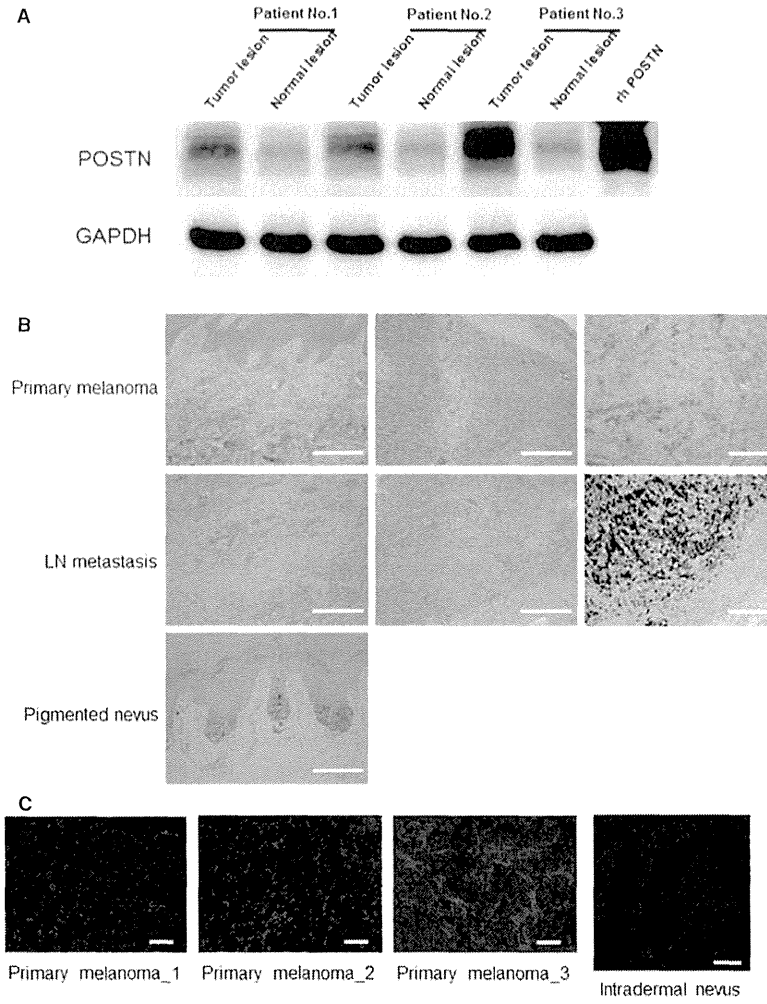

Figure 1. POSTN expression is much higher in melanoma tumor tissues compared with normal lesions. POSTN is predominantly expressed in the stroma of the melanoma tumors not melanoma cells. POSTN was slightly expressed in the in situ melanoma tissues (patient No. 1, No. 2) and highly expressed in the invasive melanoma tissues (patient No. 3) in a Western blot analysis (A). POSTN staining of invasive melanoma samples (upper three panels) and metastatic lymph nodes (middle three panels), but no expression of POSTN was detected in the pigmented nevus (lower left panel). Positive cells are stained red with ALP colorization. Bar indicates 100 μm (B). The confocal microscopic analysis showed that POSTN was strongly expressed in the stromal tissue with a lattice pattern in the 3 melanoma tissues (left 3 panels) not in the intradermal nevus (right panel). Bar indicates 20 μm for melanoma and 10 μm for intradermal nevus, respectively (C).

TGF-β1 and TGF-β3 mRNA expression in NHDFs after the coculture with melanoma cells

While the coculture of NHDF and melanoma cells was effective for the induction of POSTN expression, it was unclear how POSTN was induced during the coculture. To investigate the effect of soluble factors secreted by melanoma cells, we cultured NHDFs in the conditioned medium from MeWo or G-361 cells, and measured the expression of POSTN. However, the overexpression of POSTN was not observed at the protein level during these experiments (Figure 2E).

Next, to detect the soluble factors inducing POSTN in NHDFs, we examined the expression of POSTN-inducing cytokines, such as TGF-β1, 3, IL-4, IL-13, BMP2, and PDGF-bb, which are known to be soluble inducers of POSTN. During the RT-PCR analysis, IL-4, IL-13, BMP2, and PDGF-bb mRNA were not affected after the cocultured of melanoma cells and NHDFs (Figure 2F). However, TGF-β1 and TGF-β3 mRNA were both significantly upregulated in the cocultured NHDFs (Figure 2F). In addition, neutralization of TGF-β in the coculture markedly blocked the increase in POSTN expression (Figure 2G).

These findings indicate that cell–cell contact between NHDFs and melanoma cells is important for the expression of TGF-βs and POSTN from NHDFs, but the secretion of proteins from melanoma cells is not important for this effect.

Expression of integrin αvβ3 and αvβ5 in melanoma cells

Because integrin αvβ3, αvβ5, and α6β4 are well-known receptors for POSTN, we investigated the expression of these molecules by a Western blot analysis. We observed the expression of integrin αvβ3 and αvβ5 in the MeWo and G-361 cell lines (Figure 3A). On the other hand, integrin α6β4 was not expressed in the melanoma cells (data not shown).

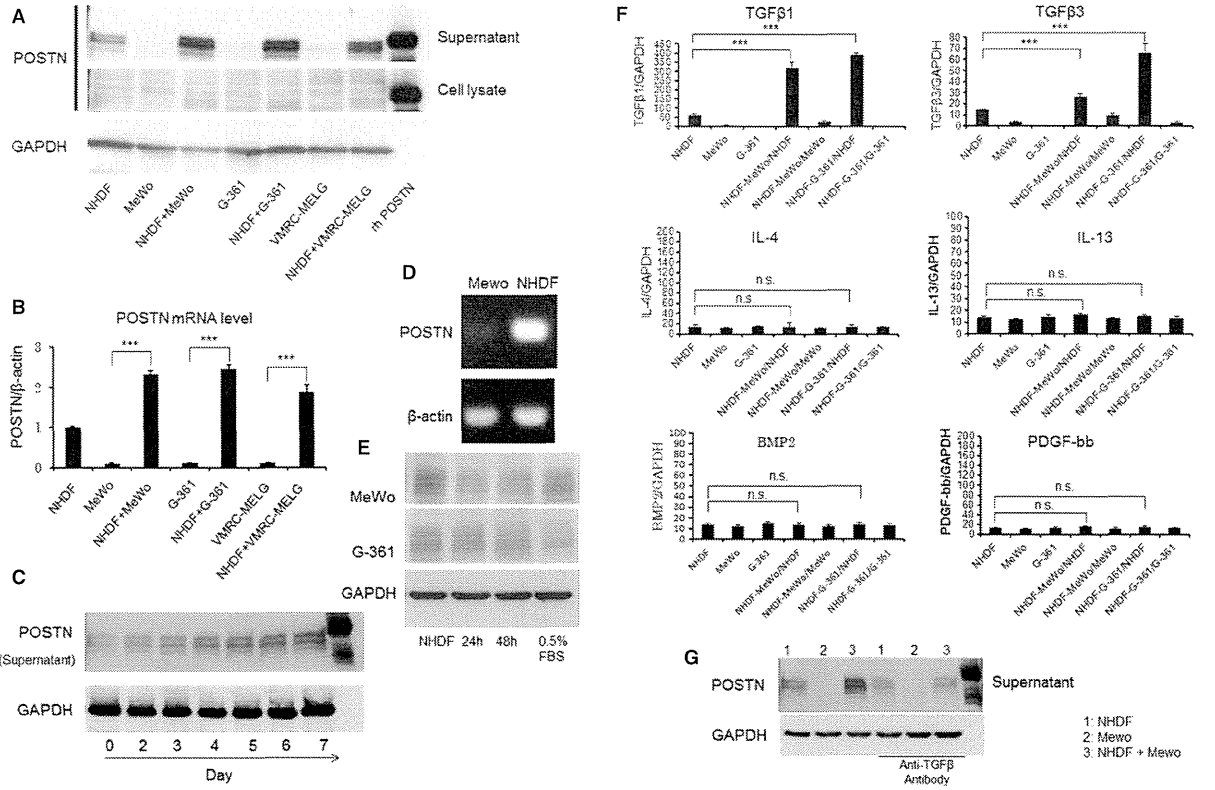

Figure 2. NHDFs secret POSTN during the coculture with human melanoma cells. The POSTN protein was upregulated in the supernatant after the coculture of NHDFs with human melanoma cells as determined by a Western blot analysis (A). POSTN mRNA was upregulated in the cell lysates after the coculture of NHDFs with human melanoma cells (B). POSTN expression was upregulated in the coculture media in a time-dependent manner (C). NHDFs, but not MeWo cells, induced POSTN expression under the coculture conditions (D). POSTN was not upregulated in the treatment with the conditioned media (E). The levels of TGFβ1, TGFβ3, IL-4, IL-13, BMP2, and PDGF-bb from NHDFs were increased after the coculture of NHDFs with melanoma cells (F). POSTN expressions were evaluated in cultured cells with or without anti-TGF-β neutralizing antibody (10 μg/ml, #MAB1835, R&D system, Minneapolis, MN). Neutralization of TGF-β blocked the increase in POSTN periostin in cocultured NHDF (G). *** indicate P-value <0.001.

Recombinant POSTN protein accelerates the proliferation of melanoma cells

To investigate the role of POSTN in the proliferation of human melanoma, we performed the MTT proliferation assay using recombinant human POSTN. The melanoma cells proliferated significantly more than control cells following the treatment with recombinant POSTN (Figure 3B). The proliferation in response to the treatment with recombinant POSTN was suppressed by anti-integrin $\alpha v\beta 3$ and $\alpha v\beta 5$ antibodies, which can neutralize the stimulation by POSTN (Figure 3C).

The phosphorylation of Akt and p44/42MAPK was observed in the cells treated with 100 ng/ml of recombinant POSTN (Figure 3D). However, the proliferation in response to the treatment with recombinant POSTN was abrogated by treatment with a MAPK inhibitor (PD98095), but not with an Akt inhibitor (LY294002) (Figure 3E). These results indicate that POSTN promotes melanoma proliferation *via* the integrin/p44/42MAPK pathway.

NHDF-derived POSTN gene transfection promotes the proliferation of melanoma cells

To investigate the role of NHDF-derived POSTN in melanoma, we transfected the NHDF-derived POSTN gene into MeWo cells (POSTN-low: lower POSTN expressing MeWo cells, POST-high: higher POSTN expressing MeWo cells, Figure 4A) and performed the MTT proliferation assay. The proliferation of POSTN–MeWo cells was significantly upregulated compared with control–MeWo (CTL-MeWo) cells in a time-dependent manner and much higher in POSTN-high cells (Figure 4B).

Significant suppression of human melanoma tumor growth in *POSTN* gene-deficient mice

We established immunodeficient Rag2 knockout mice (*Rag2* KO mice) and POSTN and Rag2 double knockout mice (*POSTN/Rag2* KO mice). We transplanted the MeWo human melanoma cell line subcutaneously onto the back of each of 17 mice and measured the tumor size for 70 days. The resulting tumors were smaller in the

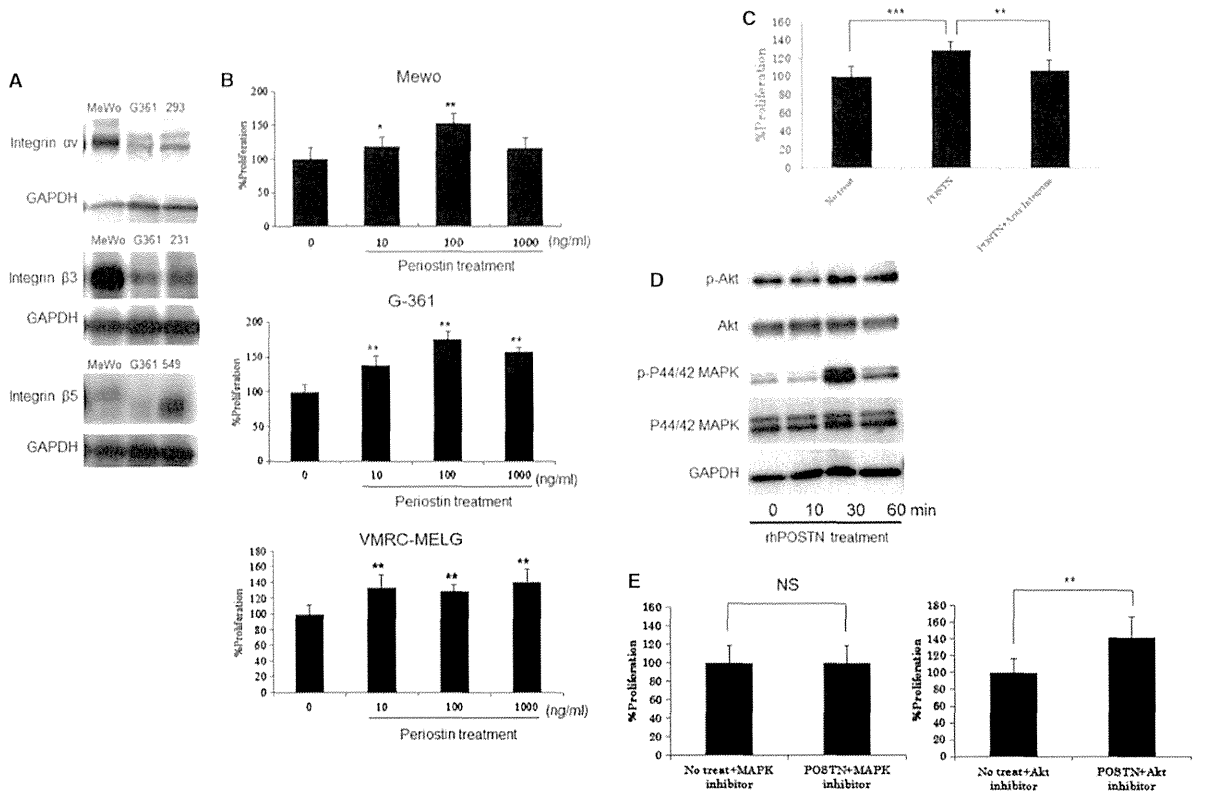

Figure 3. Recombinant POSTN protein accelerates melanoma cell proliferation via the integrin/P44/42MAPK pathway. Integrins αv, β3, and β5 were expressed in human melanoma cell lines (A). Recombinant POSTN increased the proliferation of human melanoma cells (MeWo, G-361, VMRC-MELG) (B). Neutralization of integrins αvβ3 and αvβ5 inhibited MeWo proliferation after the treatment with recombinant POSTN (C). The phosphorylation of Akt and P44/42MAPK in MeWo cells after the indicated treatment (D). Significant inhibition of MeWo cell proliferation after the treatment with recombinant POSTN by MAPK or Akt inhibitor (E). *, **, and *** indicate P-value <0.05, <0.01, <0.001, respectively.

double KO mice on day 56 after transplantation compared with the single KO mice (Figure 5A). The number of Ki-67-positive cells was significantly lower in the double KO mice compared with *Rag2* KO mice which indicated decrease in cell proliferation (Figure 5B, C). The levels of the αSMA protein, known as a marker of myofibroblasts and collagen tissue, which is colored red with E-V (Elastica van Gieson) staining, were decreased (Figure 5B). The growth of implanted melanoma tumors was also significantly suppressed in the double KO mice (Figure 5D).

Discussion

In this study, we reported the expression and function of POSTN in the ontogeny and progression of human malignant melanoma. We first noted the upregulation of POSTN protein expression in melanoma tissues compared with adjacent normal skin using an iTRAQ analysis, thereafter confirmed that higher expression in invasive melanoma. These results suggested that the upregulation of POSTN expression might be associated with the tumor malignancy. In the confocal microscopic analysis, POSTN was predominantly found to be distinctively localized in the stroma of invasive melanoma tissue, but not in cultured melanoma cells, thus suggesting the possibility that POSTN is derived from NHDFs to affect the melanoma microenvironment. The coculture of human melanoma cells with NHDFs robustly induced POSTN expression. These results indicate that POSTN expression is produced by NHDFs, but not by melanoma cells.

Recent studies have revealed that interactions between tumor cells and the surrounding stroma play an important role in facilitating tumor growth and invasion. In the present study, the induction of TGF-β in NHDF was found by melanoma cell–NHDF cell contact, and the behavior of dermal fibroblasts was altered to promote tumor growth and invasion by the interaction with surrounding melanoma cells. As reported previously, integrin was found to activate autocrine TGF-β signaling (Asano Y et al., 2005). In the present study, integrin was found highly expressed in melanoma cells (Figure 3). It suggested the similar mechanism of activated autocrine TGF-β signaling by integrin might be involved in the interaction of melanoma cell–NHDF.

Recent studies have revealed the importance of the fibrotic microenvironments surrounding cancer cells and the interactions between the host tissue and cancer cells

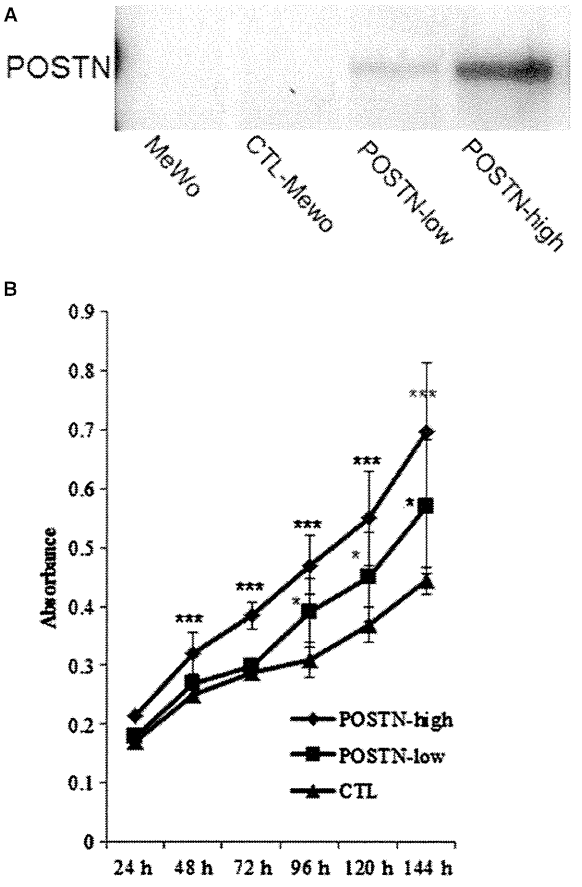

Figure 4. There is a significant increase in the proliferation of *POSTN*-transfected MeWo cells. *POSTN* gene transfection into MeWo cells (A). *POSTN* gene transfection upregulates the proliferation of MeWo cells (B). * and *** indicate P-value <0.05, <0.001, respectively.

for tumor growth and progression, because tumors are dependent on the normal host tissue-derived stromal cells and vasculature for growth and sustenance (Hanahan and Weinberg, 2000; Nyberg et al., 2008; Polyak and Kalluri, 2010; Quaranta, 2002; Yang et al., 2003; Zeisberg et al., 2002). Although there has been no previous report of a role of POSTN as stromal microenvironment in malignant melanoma, our data suggest that such a role exists.

We previously reported that POSTN accelerates dermal fibroblast proliferation, migration (Ontsuka et al., 2012), and myofibroblast differentiation, collagen 1 production (Yang et al., 2012), resulting in dermal fibrosis, and Elliott et al. also revealed the modulation of myofibroblast differentiation by POSTN (Elliott et al., 2012). These data support that NHDF-derived POSTN overexpression in the stroma of melanoma could affect the stromal microenvironment by activating dermal fibroblasts followed by tumor progression. In another report, impaired fibrous capsule formation of the implanted tumor was found in *periostin*-null mice, resulting in accelerating the tumor expansion (Guarino, 2010). Although our present data seem to be opposite of the previous report, MeWo cell established from human melanoma did not histologically form the surrounding fibrous capsule and the tumor immunity was canceled on the basis of Rag2 KO immune-deficient mice. Periostin expressed on intertumor space may be affected to accelerate adjacent melanoma cells in the present study setting.

We also revealed the proliferative effect of POSTN in human melanoma using recombinant and NHDF-derived POSTN. In details, we investigated the phosphorylation of FAK, STAT3, Akt, and p44/42MAPK, which are known to be the downstream pathways of integrin signals (Guarino, 2010). We did not observe any increase in the phosphorylation of FAK or STAT3 (data not shown), but upregulated phosphorylation of Akt and p44/42MAPK was observed after the treatment with recombinant POSTN. We also revealed that the proliferative effect of POSTN in melanoma is mediated by the integrins $\alpha v\beta 3$ and $\alpha v\beta 5$/p44/42MAPK signaling pathway, but not by the Akt pathway which is previously reported pathway (Bao et al., 2004; Ouyang et al., 2009; Yang et al., 2012).

To investigate the agonistic effect of POSTN on melanoma tissue growth in vivo, we transplanted MeWo cells into Rag2 KO mice and POSTN/Rag2 KO mice. The number of cells that were positive for Ki-67 was significantly decreased in the tumors of POSTN KO mice. In addition, the number of αSMA positive cells and the collagen expression which are known to be induced by POSTN in our previous study (Yang et al., 2012) were also decreased in POSTN KO melanomas, thus suggesting that there was suppression of the stromal microenvironment in these melanomas.

It has been reported that the POSTN expression in several cancers plays important roles in cancer progression as a result of increased proliferation, migration (Gillan et al., 2002), EMT (Soltermann et al., 2008a,b), and angiogenesis (Shao et al., 2004). In this study, our findings showed the source of POSTN to be restricted to NHDFs in human melanoma tissues, and that these stromal NHDFs between tumor cells may activate melanoma cell progression and invasion through an enhanced deposition of POSTN in the melanoma microenvironment.

Recent advances in the therapeutic approach for advanced melanoma have led to many clinical trials for patients with melanoma. For example, a BRAF inhibitor was reported to dramatically improve the prognosis of patients with melanoma. However, it was only effective in patients with the *V600E* gene mutation in the tyrosine kinase site (Atefi et al., 2011; Flaherty et al., 2010). Treatment with an anti-CTLA4 antibody can augment the anti-tumor immune response against melanoma tissue by blocking the immune-attenuating molecule, CTLA4, in T cells. However, the administration of the CTLA4 antagonist can induce severe autoimmune reactions, such as colitis and skin rashes (Weber, 2008). Therefore, it is essential to look for other therapeutic modalities with

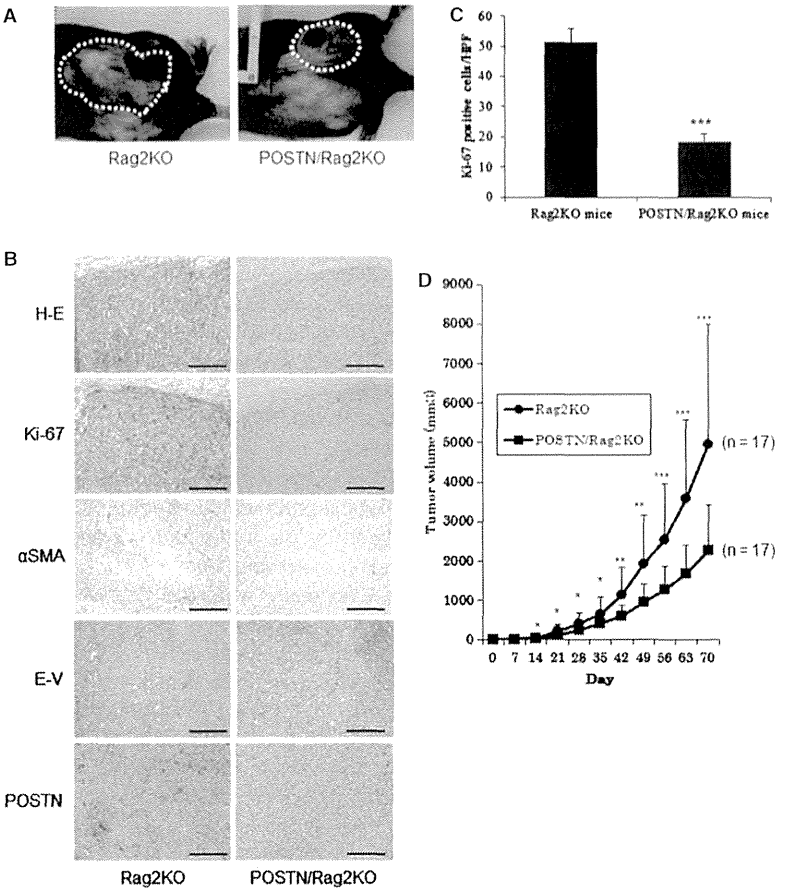

Figure 5. Melanoma tumorigenesis is significantly suppressed in *POSTN* gene knockout mice. Macroscopic feature of the *Rag2* KO and *POSTN/Rag2* KO mice on the day 56 after human melanoma cell implantation (A). There was decreased expression of Ki-67, αSMA, and collagen in the tumors of *POSTN/Rag2* KO mice. Dermal myofibroblast is positive for αSMA staining and collagen tissue becomes red by E-V (Elastica van Gieson) staining. Bar indicates 250 μm (B). There was a significant decrease in the number of Ki-67-positive cells in *POSTN/Rag2* KO mice (C). There was significant suppression of melanoma tumorigenesis in *POSTN* gene knockout mice (D). *, **, and *** indicate P-value <0.05, <0.01, <0.001, respectively.

novel mechanism(s) of action, which are not associated with such life-threatening adverse events. We believe that POSTN is important for the growth of melanoma, because the implanted melanoma cell grew more slowly in *POSTN*-depleted mice compared with matched control mice. A therapeutic approach targeting POSTN and its related signaling may lead to a safer treatment for malignant melanoma, and one that is less likely to be thwarted by resistance of the cancer cells.

In this experimental setting, there was no significant improvement in the overall survival in the POSTN-depleted mice even though the tumor growth was attenuated in KO mice compared with control mice on an immune-deficient background. There is no doubt that the survival is strongly dependent on the metastasis of the inoculated tumor cells, but we did not observe any metastasis in either the KO or wild-type mice, which likely contributed to the lack of a difference in the overall survival between the groups.

In conclusion, in human melanoma tissue, NHDFs interacted with melanoma cells to induce POSTN, which directly promoted melanoma cell proliferation by activating integrin/p44/42MAPK signals and indirectly instituted a fibrotic microenvironment in the tumor, thus resulting in a progression of the melanoma. As a result, the suppression of POSTN represents a novel therapeutic target for cutaneous malignant melanoma.

Methods

Cells and tissue samples

Human melanoma cell lines (MeWo, G-361, and VMRC-MELG) were obtained from the Japanese Collection of Research Bioresources (JCRB, Osaka, Japan), and NHDFs were obtained from TaKaRa Bio (Shiga, Japan). 293, 231, and A549 were represented by HEK293, MDA-MB-231, and A549 cancer cell lines loaded as positive controls, respectively (JCRB). All melanoma and normal tissue samples were obtained from patients at Osaka University Hospital (Department of Dermatology, Osaka, Japan). All clinical samples were collected after approval was obtained from the local ethics committee, and informed consent was obtained from each patient for use of the samples. Details of cell culture are described in Data S1.

Mice

Twelve-week-old Rag2-deficient (*Rag2*$^{-/-}$, C57BL/6 background) and periostin-deficient (*Postn*$^{-/-}$, C57BL/6 background) mice were used for the studies (Shimazaki et al., 2010). Experiments were undertaken following the guidelines for the care and use of experimental animals as required by the Japanese Association for Laboratory Animals Science (1987).

Sample preparation and iTRAQ labeling

Proteins were extracted from the frozen tumor and normal skin tissue samples. Details are described in Data S1.

Extracted proteins were purified using a 2D clean-up kit (GE Healthcare, Buckinghamshire, UK). Subsequently, 100 μg of each protein was dissolved, reduced, alkylated, and digested with trypsin, according to the manufacturer's protocol (Applied Biosystems, Foster City, CA, USA). The samples were labeled with iTRAQ reagent: reagent 114 for melanoma in situ, reagent 115 for normal skin lesions of melanoma in situ, reagent 116 for invasive melanoma, and reagent 117 for normal skin lesions of invasive melanoma. The labeled peptide samples were mixed and fractionated as described previously (Serada et al., 2010).

Mass spectrometric analysis and iTRAQ data analysis

NanoLC-MS/MS analyses and iTRAQ data analysis were performed as described in Data S1.

Western blot analysis

Cell lysates and supernatant fluids were used for the Western blot analyses. Details were described in Data S1.

Immunohistochemistry

Patient with paraffin-embedded melanoma tissue sections and in vivo mice melanoma tissue sections were stained with hematoxylin and eosin (H&E). For the immunohistochemical analysis, primary antibodies were used at the following dilutions: the human and mouse anti-POSTN (1:3000; Abcam, Tokyo, Japan), mouse anti-Ki-67 (1:500; Novocastra Laboratories Ltd, Newcastle, UK), and mouse anti-α-smooth muscle actin (α-SMA; 1:3000 dilution; Sigma-Aldrich, St. Louis, MO, USA). Details are described in Data S1.

Reverse transcription polymerase chain reaction (RT-PCR) analysis

To confirm the altered expression of POSTN in melanoma cells and NHDFs, melanoma cells (MeWo, G-361, and VMRC-MELG), NHDFs, and the cocultured cell samples were subjected to RT-PCR. β-actin was used as a housekeeping gene to evaluate and compare the quality of different cDNA samples. The primer sequences and the expected sizes of PCR products were as follows:

periostin, forward, 5′-TTGAGACGCTGGAAGGAAAT-3′
reverse, 5′-AGATCCGTGAAGGTGGTTTG-3′ (199 bp);
β-actin, forward, 5′-AGCCTCGCCTTTGCCGA-3′
reverse, 5′-CTGGTGCCTGGGGCG-3′(174 bp);

Details of total RNA extraction, quantitect reverse transcription, and RT-PCR are described in Data S1.

Quantitative reverse transcription polymerase chain reaction (qT-PCR) analysis

Normal human dermal fibroblasts were cocultured with CFSE-labeled MeWo and G-361 cells for 24 h. Thereafter, we sorted these cells into NHDF, MeWo, and G-361 cells using a FACS system. Next, the total RNA was isolated from the sorted NHDF, MeWo, and G-361 cells, and the products were reverse-transcribed into cDNA. The expression of TGFβ1, TGFβ3, IL-4, IL-13, BMP2, and PDGF-bb was measured using the Power SYBR Green PCR Master Mix (Applied Biosystems, Tokyo, Japan) according to the manufacturer's protocol. Glyceraldehyde-3-phosphate dehydrogenase (GAPDH) was used to normalize the mRNA, as GAPDH was not affected by the treatment. The primer sequences used were as follows:

TGFβ1, forward, 5′-TCGCCAGAGTGGTTATCTTTTG-3′
reverse, 5′-AGGAGCAGTGGGCGCTAAG-3′;
TGFβ3, forward, 5′-GCCCTTGCCCATACCTCCGC-3′
reverse, 5′-CGCAGCAAGGCGAGGCAGAT-3′;
GAPDH, forward, 5′-GGAGTCAACGGATTTGGTCGTA-3′
reverse, 5′-GCAACAATATCCACTTTACCAGAGTTAA-3′;
IL-4, forward, 5′-ACATTGTCACTGCAAATCGACACC-3′
reverse, 5′-TGTCTGTTACGGTCAACTCGGTGC-3′;
IL-13, forward, 5′-GCAATGGCAGCATGGTATGG-3′
reverse, 5′-AAGGAATTTTACCCCTCCCTAACC-3′;
BMP2, forward, 5′-ACTCGAAATTCCCCGTGACC-3′
reverse, 5′-CCACTTCCACCACGAATCCA-3′;
PDGF-bb, forward, 5′-CAGCGCCCATTTTTCATTCC-3′
reverse, 5′-GTTTTCTCTTTGCAGCGAGGC-3′.

Construction of a NHDF-derived POSTN expression vector

To construct a NHDF-derived POSTN expression vector, the cDNA of human POSTN derived from NHDFs cocultured with melanoma cells was amplified. The amplified cDNA was then inserted into the pcDNA3.1/V5-His-TOPO vector (Invitrogen, Carlsbad, CA, USA) and designated pcDNA3.1-POSTN.

Generation of NHDF-derived POSTN stable transfectant melanoma cells

To generate NHDF-derived POSTN stable transfectant cells (POSTN–MeWo), the MeWo cell line was transfected with pcDNA3.1-POSTN using Lipofectamine 2000 (Invitrogen) according to the manufacturer's instructions, after which the cells were selected with 500 μg/ml of Geneticin (GIBCO; Invitrogen). Stable clones were maintained in 250 μg/ml of Geneticin.

Proliferation assay

The proliferation of MeWo, G-361, VMRC-MELG, and POSTN–MeWo melanoma cells was examined using the Cell Counting Reagent SF (Nacalai Tesque, Kyoto, Japan) according to the manufacturer's recommendations, and then, absorbance was measured with a microplate reader (model 680; Bio-Rad, Tokyo, Japan) at test and reference wavelengths of 450 and 630 nm, respectively.

Kinase inhibition assays

The cells were incubated for 2 h with kinase inhibitors (Cell Signaling Technology, Beverly, MA, USA): LY294002 (10 μM) as an Akt inhibitor and PD98095 (10 μM) as a MAPK inhibitor. Cells were then stimulated with 100 ng/ml of recombinant POSTN in the same media. After stimulation, the MTT proliferation assay was performed.

Statistical analyses

The results are presented as the means + SD. The analyses were carried out using the two-sided, unpaired Student's *t* test or the two-sided Welch test. Multiple comparisons between groups were made by Fisher's or Dunnett's methods. We considered values to be significant when $P < 0.05$.

Acknowledgements

This study was supported by a Grant-in-Aid for Young Scientists (B) (22791100) from the Japanese Ministry of Education, Science, Sports, and Culture; a Grant-in-Aid for the Program for Promotion of Fundamental Studies in Health Sciences of the National Institute of Biomedical Innovation; and a Grant-in-Aid from the Ministry of Health, Labour, and Welfare of Japan.

Disclosure statement

All authors declare no financial support or relationship that may pose conflict of interest.

References

Asano Y, I.H., Yamane K, J.M., Mimura, Y., and Tamaki, K. (2005). Increased expression of integrin alpha(v)beta3 contributes to the establishment of autocrine TGF-beta signaling in scleroderma fibroblasts. J. Immunol. *175*, 7708–7718.

Atefi, M., von Euw, E., Attar, N. et al. (2011). Reversing melanoma cross-resistance to BRAF and MEK inhibitors by co-targeting the AKT/mTOR pathway. PLoS ONE *6*, e28973.

Bao, S., Ouyang, G., Bai, X. et al. (2004). Periostin potently promotes metastatic growth of colon cancer by augmenting cell survival via the Akt/PKB pathway. Cancer Cell *5*, 329–339.

Baril, P., Gangeswaran, R., Mahon, P.C. et al. (2007). Periostin promotes invasiveness and resistance of pancreatic cancer cells to hypoxia-induced cell death: role of the beta4 integrin and the PI3k pathway. Oncogene *26*, 2082–2094.

Elliott, C.G., Wang, J., Guo, X. et al. (2012). Periostin modulates myofibroblast differentiation during full-thickness cutaneous wound repair. J. Cell Sci. *125*, 121–132.

Erkan, M., Kleeff, J., Gorbachevski, A. et al. (2007). Periostin creates a tumor-supportive microenvironment in the pancreas by sustaining fibrogenic stellate cell activity. Gastroenterology *132*, 1447–1464.

Flaherty, K.T., Puzanov, I., Kim, K.B. et al. (2010). Inhibition of mutated, activated BRAF in metastatic melanoma. N. Engl. J. Med. *363*, 809–819.

Gillan, L., Matei, D., Fishman, D.A., Gerbin, C.S., Karlan, B.Y., and Chang, D.D. (2002). Periostin secreted by epithelial ovarian carcinoma is a ligand for alpha(V)beta(3) and alpha(V)beta(5) integrins and promotes cell motility. Cancer Res. *62*, 5358–5364.

Guarino, M. (2010). Src signaling in cancer invasion. J. Cell. Physiol. *223*, 14–26.

Hanahan, D., and Weinberg, R.A. (2000). The hallmarks of cancer. Cell *100*, 57–70.

Horiuchi, K., Amizuka, N., Takeshita, S. et al. (1999). Identification and characterization of a novel protein, periostin, with restricted expression to periosteum and periodontal ligament and increased expression by transforming growth factor beta. J. Bone Miner. Res. *14*, 1239–1249.

Inai, K., Norris, R.A., Hoffman, S., Markwald, R.R., and Sugi, Y. (2008). BMP-2 induces cell migration and periostin expression during atrioventricular valvulogenesis. Dev. Biol. *315*, 383–396.

Kudo, Y., Ogawa, I., Kitajima, S. et al. (2006). Periostin promotes invasion and anchorage-independent growth in the metastatic process of head and neck cancer. Cancer Res. *66*, 6928–6935.

Li, J.S., Sun, G.W., Wei, X.Y., and Tang, W.H. (2002). Expression of periostin and its clinicopathological relevance in gastric cancer. World J. Gastroenterol. *13*, 5261–5266.

Li, G., Oparil, S., Sanders, J.M. et al. (2006). Phosphatidylinositol-3-kinase signaling mediates vascular smooth muscle cell expression of periostin in vivo and in vitro. Atherosclerosis *188*, 292–300.

Nyberg, P., Salo, T., and Kalluri, R. (2008). Tumor microenvironment and angiogenesis. Front Biosci. *13*, 6537–6553.

Ontsuka, K., Kotobuki, Y., Shiraishi, H. et al. (2012). Periostin, a matricellular protein, accelerates cutaneous wound repair by activating dermal fibroblasts. Exp. Dermatol. *21*, 331–336.

Ouyang, G., Liu, M., Ruan, K., Song, G., Mao, Y., and Bao, S. (2009). Upregulated expression of periostin by hypoxia in non-small-cell lung cancer cells promotes cell survival via the Akt/PKB pathway. Cancer Lett. *281*, 213–219.

Polyak, K., and Kalluri, R. (2010). The role of the microenvironment in mammary gland development and cancer. Cold Spring Harb. Perspect. Biol. *2*, a003244.

Puppin, C., Fabbro, D., Dima, M. et al. (2008). High periostin expression correlates with aggressiveness in papillary thyroid carcinomas. J. Endocrinol. *197*, 401–408.

Quaranta, V. (2002). Motility cues in the tumor microenvironment. Differentiation *70*, 590–598.

Riener, M.O., Fritzsche, F.R., Soll, C. et al. (2010). Expression of the extracellular matrix protein periostin in liver tumours and bile duct carcinomas. Histopathology *56*, 600–606.

Sasaki, H., Dai, M., Auclair, D. et al. (2001). Serum level of the periostin, a homologue of an insect cell adhesion molecule, as a prognostic marker in nonsmall cell lung carcinomas. Cancer *92*, 843–848.

Sasaki, H., Sato, Y., Kondo, S. et al. (2002). Expression of the periostin mRNA level in neuroblastoma. J. Pediatr. Surg. *37*, 1293–1297.

Sasaki, H., Yu, C.Y., Dai, M. et al. (2003). Elevated serum periostin levels in patients with bone metastases from breast but not lung cancer. Breast Cancer Res. Treat. *77*, 245–252.

Serada, S., Fujimoto, M., Ogata, A. et al. (2010). iTRAQ-based proteomic identification of leucine-rich alpha-2 glycoprotein as a novel inflammatory biomarker in autoimmune diseases. Ann. Rheum. Dis. *69*, 770–774.

Shao, R., Bao, S., Bai, X. et al. (2004). Acquired expression of periostin by human breast cancers promotes tumor angiogenesis through up-regulation of vascular endothelial growth factor receptor 2 expression. Mol. Cell. Biol. *24*, 3992–4003.

Shimazaki, M., Nakamura, K., Kii, I. et al. (2010). Periostin is essential for cardiac healing after acute myocardial infarction. J. Exp. Med. *205*, 295–303.

Soltermann, A., Ossola, R., Kilgus-Hawelski, S. et al. (2008a). N-glycoprotein profiling of lung adenocarcinoma pleural effusions by shotgun proteomics. Cancer *114*, 124–133.

Soltermann, A., Tischler, V., Arbogast, S. et al. (2008b). Prognostic significance of epithelial-mesenchymal and mesenchymal-epithelial transition protein expression in non-small cell lung cancer. Clin. Cancer Res. *14*, 7430–7437.

Takayama, G., Arima, K., Kanaji, T. et al. (2006). Periostin: a novel component of subepithelial fibrosis of bronchial asthma downstream of IL-4 and IL-13 signals. J. Allergy Clin. Immunol. *118*, 98–104.

Takeshita, S., Kikuno, R., Tezuka, K., and Amann, E. (1993). Osteoblast-specific factor 2: cloning of a putative bone adhesion protein with homology with the insect protein fasciclin I. Biochem. J. *294*(Pt 1), 271–278.

Tilman, G., Mattiussi, M., Brasseur, F., van Baren, N., and Decottignies, A. (2007). Human periostin gene expression in normal tissues, tumors and melanoma: evidences for periostin production by both stromal and melanoma cells. Mol. Cancer. *6*, 80.

Tischler, V., Fritzsche, F.R., Wild, P.J. et al. (2010). Periostin is up-regulated in high grade and high stage prostate cancer. BMC Cancer *10*, 273.

Weber, J. (2008). Overcoming immunologic tolerance to melanoma: targeting CTLA-4 with ipilimumab (MDX-010). Oncologist *13*(Suppl 4), 16–25.

Yan, W., and Shao, R. (2006). Transduction of a mesenchyme-specific gene periostin into 293T cells induces cell invasive activity through epithelial-mesenchymal transformation. J. Biol. Chem. *281*, 19700–19708.

Yang, C., Zeisberg, M., Lively, J.C., Nyberg, P., Afdhal, N., and Kalluri, R. (2003). Integrin alpha1beta1 and alpha2beta1 are the key regulators of hepatocarcinoma cell invasion across the fibrotic matrix microenvironment. Cancer Res. *63*, 8312–8317.

Yang, L., Serada, S., Fujimoto, M. et al. (2012). Periostin facilitates skin sclerosis via PI3K/Akt dependent mechanism in a mouse model of scleroderma. PLoS ONE *7*, e41994.

Zeisberg, M., Maeshima, Y., Mosterman, B., and Kalluri, R. (2002). Renal fibrosis. Extracellular matrix microenvironment regulates migratory behavior of activated tubular epithelial cells. Am. J. Pathol. *160*, 2001–2008.

Supporting information

Additional Supporting Information may be found in the online version of this article:

Table S1. List of all proteins identified by iTraq.

Data S1. Methods.

Cancer Chemother Pharmacol (2014) 74:629–636
DOI 10.1007/s00280-014-2521-x

CLINICAL TRIAL REPORT

Phase I dose-escalation study of the HSP90 inhibitor AUY922 in Japanese patients with advanced solid tumors

Toshihiko Doi · Yusuke Onozawa · Nozomu Fuse · Takayuki Yoshino · Kentaro Yamazaki · Junichiro Watanabe · Mikhail Akimov · Matthew Robson · Narikazu Boku · Atsushi Ohtsu

Received: 2 June 2014 / Accepted: 3 July 2014 / Published online: 25 July 2014

Abstract
Purpose AUY922 is a potent non-geldanamycin inhibitor of heat-shock protein 90. This study was carried out in Japanese patients to determine the maximum tolerated dose (MTD), and to characterize safety, tolerability and pharmacokinetics of single-agent AUY922.
Methods Japanese patients with advanced solid tumors whose disease had progressed on at least one line of standard therapy, or for whom no standard therapy existed, were treated with AUY922 (intravenous, once-weekly, 28-day cycle, starting dose 8 mg/m^2).
Results Thirty-one patients were treated. Two DLTs were reported in one patient of the 54 mg/m^2 cohort; fatigue and decreased appetite (both Grade 3, resolving to Grade 1 within 8 days). No MTD was determined, and the dose recommended for Phase II studies was determined to be 70 mg/m^2 once-weekly. Most common drug-related toxicities were diarrhea, night blindness and nausea. Grade 1 and 2 visual toxicities at high AUY922 doses $\geq$22 mg/m^2 were observed. Ten patients (32 %) achieved a best overall response of stable disease, and one patient (3 %) achieved a confirmed partial response.
Conclusion Overall, AUY922 exhibited acceptable toxicities and demonstrated potential clinical activity in Japanese patients, with similar safety and pharmacokinetic profiles to those reported in a preceding global Phase I study in Western patients (CAUY922A2101).

Keywords AUY922 · Clinical trial · HSP90 · Japanese · Phase I

T. Doi (✉) · N. Fuse · T. Yoshino · A. Ohtsu
National Cancer Center Hospital East, 6-5-1 Kashiwanoha, Kashiwa, Chiba 277-8577, Japan
e-mail: tdoi@east.ncc.go.jp

Y. Onozawa · K. Yamazaki · J. Watanabe · N. Boku
Shizuoka Cancer Center, 1007 Shimonagakubo, Nagaizumi-cho, Sunto-gun, Shizuoka 411-8777, Japan

M. Akimov
Novartis Pharma AG, 4002, Novartis Campus, Basel, Switzerland

M. Robson
Novartis Pharma K.K., 4-12-24, Nishi-azabu, Minato-ku, Tokyo 106-0031, Japan

Introduction

Heat-shock proteins (HSPs) are molecular chaperones that assist in the structural formation, folding and activation of a wide variety of oncogenic client proteins involved in diverse cellular processes such as apoptosis, proliferation, signal transduction and transcription control [1–4]. These client proteins include human epidermal growth factor receptor 2 (HER2), estrogen receptor, epidermal growth factor receptor, platelet-derived growth factor receptor, vascular endothelial growth factor, AKT, c-KIT and c-MET [1, 2]. HSP90 is the most abundant molecular chaperone and is essential for cell survival, proliferation and apoptosis. These processes are significantly affected by HSP90 inhibition, and therefore, HSP90 inhibitors are considered to have a strong therapeutic potential in a wide variety of tumor types [5]. Indeed, HSP90 inhibitors degrade a variety of oncogenic client proteins [6–8]. In addition, HSP90 inhibitors show synergy with various chemotherapeutic agents in murine tumor models and sensitize tumor cells to their cytotoxic effects [6–8].

AUY922 (5-[2,4-dihydroxy-5-isopropyl-phenyl]-*N*-ethyl-4-[4-(morpholinomethyl) phenyl]isoxazole-3-carboxamide)

is a highly potent, isoxazole-based, non-geldanamycin HSP90 inhibitor that inhibits the ATPase activity of HSP90, and leads to misfolding of client proteins [9, 10]. AUY922 has significant antitumor activity in a wide range of cancer cell lines and inhibits tumor growth in murine xenograft models [9–13]. In a preceding global Phase I study in Western patients (CAUY922A2101), the recommended Phase II dose (RP2D) of AUY922 was determined to be 70 mg/m^2 intravenous (IV) once-weekly [14]. Phase II studies have been initiated in patients with HER2-positive breast cancer, gastric cancer and non-small cell lung cancer to further investigate the safety profile and clinical efficacy of AUY922 as a single agent and in combination with other agents. In these global Phase II studies, AUY922 was well tolerated with promising clinical activity as single-agent therapy, as well as in combination with other agents, in some sub-populations with actively progressing disease [15, 16].

In the present open-label, Phase I dose-escalation study, the safety, pharmacokinetics (PK) and clinical efficacy of AUY922 were evaluated in Japanese patients with advanced solid tumors. The primary objective was to determine the maximum tolerated dose (MTD) of AUY922 as a single agent when administered intravenously on a once-weekly schedule. Secondary objectives were to characterize the safety and tolerability of AUY922 treatment, evaluate the preliminary antitumor activity of AUY922 as a single agent and observe the PK profile of AUY922 and its metabolite.

Materials and methods

Patient population

Adult patients (aged ≥20 years) with histologically confirmed, advanced solid tumors whose disease had progressed on at least one line of standard systemic therapy, or for whom no standard therapy existed, were eligible. Inclusion criteria included Eastern Cooperative Oncology Group performance status ≤2 and life expectancy ≥12 weeks. Laboratory parameters required were absolute neutrophil count ≥1.5 × 10^9/l, hemoglobin ≥8.5 g/dl, platelets ≥100 × 10^9/l, potassium, calcium, magnesium, phosphorus within normal limits or correctable with supplements, aspartate aminotransferase and alanine aminotransferase ≤2.5 × upper limit of normal (ULN), serum bilirubin ≤1.5 × ULN, serum albumin >2.5 g/dl, and serum creatinine ≤1.5 × ULN or 24-hour clearance ≥50 ml/min.

Exclusion criteria included central nervous system metastases, acute or chronic liver or renal disease and previous treatment with histone deacetylase or HSP90 inhibitors. Patients were excluded who had clinically significant heart disease, QTc ≥450 ms on screening electrocardiogram (ECG), ischemic heart disease, heart failure, ECG abnormalities, atrial fibrillation, atrial flutter or ventricular arrhythmias including ventricular tachycardia or Torsades de Pointes, or a history (or family history) of long QT syndrome. Patients receiving any medication that had a risk of prolonging the QTcF interval or inducing Torsades de Pointes, and those with disorders known to be caused by a deficiency in bilirubin glucuronidation (e.g., Gilbert's syndrome), were also excluded.

This trial was conducted in accordance with the Declaration of Helsinki and the Good Clinical Practice guidelines (Japanese Ministry of Health, Labour and Welfare). All studies were performed after approval by local ethical committee/institutional review board. Written informed consent was obtained from all patients before screening.

Dosing and administration

AUY922 was administered by IV infusion over 1 h, once every week (Days 1, 8, 15 and 22) until disease progression, unacceptable toxicity, or withdrawal by investigator decision or patient refusal. The starting dose was 8 mg/m^2, and treatment cycles were 28 days. Intra-patient dose escalation was not permitted. An adaptive Bayesian logistic regression model (BLRM), guided by the escalation with overdose control (EWOC) principle, was used to guide dose escalations [17]. The EWOC principle mandates the potential doses recommended for the next cohort and the estimated MTD have less than 25 % posterior probability of DLT in the excessive toxicity interval (33, 100 %). The information about dose-limiting toxicity (DLT) available from the CAUY922A2101 study at the time of the start of this study supported a starting dose of 8 mg/m^2 [50 % of the highest dose (16 mg/m^2) associated with no DLTs]. Toxicities at both the 8 and 16 mg/m^2 dose levels in that study had been mild, and the preliminary PK results had shown no accumulation of the drug up to a dose of 16 mg/m^2. The occurrence of DLTs was evaluated during Cycle 1. A minimum of three patients were enrolled in a cohort, and the estimated MTD was continuously updated using the BLRM, and a minimum of six patients were planned to be enrolled at the MTD level. The final recommended dose was based on overall safety assessments and MTD estimated by the BLRM, which was the dose of AUY922 with the highest posterior probability of DLT in the target interval (16, 33 %) among the doses fulfilling the EWOC principle [18]. A minimum of 15 patients were required for the BLRM model to determine the MTD. AUY922 was supplied as 10-ml ampoules of a 5-mg/ml solution, which was diluted into 5 % dextrose or glucose to a maximum infusion volume of 500 ml, under aseptic conditions and protected from light to prevent the photolabile drug from

Table 1 Patient demographics, and baseline disease characteristics

Characteristic	AUY922 dose (mg/m^2)							
	8 ($n = 3$)	16 ($n = 3$)	22 ($n = 3$)	28 ($n = 5$)	40 ($n = 3$)	54 ($n = 6$)	70 ($n = 8$)	Total, n (%) ($N = 31$)
Mean age, years	51.3	61.7	52.7	53.6	62.0	62.3	59.4	58.1
Gender, n								
Male	2	1	3	2	1	2	4	15 (48)
ECOG PS, n								
0	2	3	2	3	3	4	4	21 (68)
1	1	0	1	2	0	2	4	10 (32)
Stage (current), n								
IV	3	3	3	3	3	6	8	29 (94)
IVa	0	0	0	1	0	0	0	1 (3)
IVb	0	0	0	1	0	0	0	1 (3)
Tumor type, n								
Rectum	0	10	2	0	0	2	5	10 (32)
Colon	1	1	1	0	1	2	1	7 (23)
Breast	0	0	0	2	1	1	1	5 (16)
Head and neck	1	0	0	0	1	0	0	2 (7)
Pancreas	0	0	0	1	0	0	1	2 (7)
Stomach	1	1	0	0	0	0	0	2 (7)
Eesophagus	0	0	0	1	0	0	0	1 (3)
Gall bladder ducts	0	0	0	1	0	0	0	1 (3)
Other	0	0	0	0	0	1	0	1 (3)

ECOG PS Eastern Cooperative Oncology Group performance status

decomposition. Doses were individually adjusted according to body surface area measured at baseline.

Safety assessments

Toxicity was graded according to the National Cancer Institute Common Toxicity Criteria version 3.0. DLTs were defined as clinically relevant adverse events (AEs; mainly Grade 3 or 4) or abnormal laboratory values, occurring within 28 days following the first dose of AUY922 in Cycle 1. Tumor response was assessed by computed tomography or magnetic resonance imaging, and using Response Evaluation Criteria in Solid Tumors version 1.0 for efficacy evaluations.

Based on reports of Grade 1–3 visual symptoms after weekly administration of AUY922 at dose levels of $\geq$40 mg/m^2 in the CAUY922A2101 study, standard ophthalmological assessments were implemented at baseline, at the time of reported visual symptom(s) (if any) and at the end of treatment.

Pharmacokinetic analysis

Validated liquid chromatography-tandem mass spectrometry assay was used for PK assessments of AUY922 and its glucuronide metabolite BJP762. PK assessments were carried out on blood samples obtained pre-infusion and at 5, 15, and 30 min and 1 h during infusion, followed by 5 and 30 min and 1, 2, 4, 5, 8, 24, 48 and 72-h post-infusion on Cycle 1 Day 1 and Cycle 2 Day 1. A non-compartmental analytical method was used to calculate PK parameters of maximum observed concentration (C_{max}), time at which C_{max} occurred (T_{max}), terminal half-life ($T_{1/2}$), and area under the curve (AUC), for AUY922 and BJP762 in blood, utilizing WinNonlin Pro version 5.2.

Results

Patient characteristics and treatment

A total of 31 patients were treated in seven dose cohorts (8, 16, 22, 28, 40, 54 and 70 mg/m^2) between November 2008 and July 2011 (Table 1). Median duration of drug exposure was 7.3 weeks (range 0.1–58.1 weeks) and 55 % of patients underwent 1 or 2 treatment cycles [7 patients (23 %) and 10 patients (32 %), respectively]. The median relative dose intensity was 1.0 (range 0.7–1.0). At the time of data cut-off (5 July 2011), two patients were still receiving treatment on the study. The remaining 29 patients discontinued

Table 2 Most common adverse events (≥10 % and Grade 3/4) potentially related to AUY922 treatment

Adverse event, n[a]	Grade	AUY922 dose (mg/m^2)							
		8 ($n = 3$)	16 ($n = 3$)	22 ($n = 3$)	28 ($n = 5$)	40 ($n = 3$)	54 ($n = 6$)	70 ($n = 8$)	Total, n (%) ($N = 31$)
Diarrhea	All	0	0	2	4	2	5	7	20 (65)
	3/4	0	0	0	0	0	1	0	1 (3)
Night blindness	All	0	0	2	2	1	5	3	13 (42)
	3/4	0	0	0	0	0	0	0	0
Nausea	All	0	0	0	0	2	2	3	7 (23)
	3/4	0	0	0	0	0	0	0	0
Decreased appetite	All	0	1	1	0	0	1	3	6 (19)
	3/4	0	0	0	0	0	1	0	1 (3)
Fatigue	All	0	0	0	2	0	3	1	6 (19)
	3/4	0	0	0	0	0	1	0	1 (3)
Rash	All	0	2	0	1	0	2	1	6 (19)
	3/4	0	0	0	0	0	0	0	0
Vomiting	All	0	0	0	0	1	1	3	5 (16)
	3/4	0	0	0	0	0	0	0	0
Headache	All	0	0	0	0	0	0	3	3 (10)
	3/4	0	0	0	0	0	0	0	0
Lymphopenia	All	0	0	0	2	0	1	0	3 (10)
	3/4	0	0	0	0	0	0	0	0
Photopsia	All	0	0	1	1	0	0	1	3 (10)
	3/4	0	0	0	0	0	0	0	0
Pruritis	All	0	1	0	0	0	1	1	3 (10)
	3/4	0	0	0	0	0	0	0	0

Patients who experienced more than one occurrence of the same event are only counted once within each category

[a] By preferred term

the study treatment, mainly due to disease progression (27 patients), and two patients discontinued as a result of AEs related to study drug (one patient each in the 54 and 70-mg/m^2 cohorts).

Safety and tolerability

The most common AEs, regardless of relationship to study drug, were diarrhea (65 %), night blindness (42 %), nausea and fatigue (both 29 %). Mild-to-moderate diarrhea (65 %), night blindness (42 %) and nausea (23 %) were the most commonly reported AEs possibly related to AUY922 treatment across all doses (Table 2). Visual toxicities, including night blindness, photopsia, cataract, eye disorder, optic neuritis and blurred vision were observed at dose levels of 22–70 mg/m^2; all were Grade 1 or 2. No patients discontinued AUY922 treatment due to the visual toxicities, which were reversible upon discontinuation of treatment. None of the visual AEs were reported as DLTs. Fifteen patients (48 %) experienced AEs requiring dose modification or interruption. Of these, night blindness (six patients) and eye disorder (two patients) were reported. Eight patients (26 %) experienced serious AEs (SAEs) and SAEs considered to be related to the study drug were reported in two patients. One patient died during the study as a result of disease progression, which was considered to be unrelated to study drug.

The dose-determining set (DDS) consisted of (1) all patients who received at least three doses of AUY922 within the first cycle, were observed for ≥28 days following the first dose, and completed all safety evaluations in Cycle 1, or (2) any patient who had a DLT within Cycle 1. The DDS was used for the BLRM analyses in the determination of MTD. Among these patients ($n = 28$), one patient (3.6 %) in the 54-mg/m^2 cohort experienced DLTs; two AEs (Grade 3 fatigue and Grade 3 decreased appetite) were considered to be DLTs and both resolved to Grade 1 within 8 days. Two patients who received the 70 mg/m^2 dose required repeated dose interruption due to visual adverse events, and both patients ultimately received a dose reduction to 54 mg/m^2. Although the BLRM would have permitted dose escalation beyond 70 mg/m^2, a decision to stop further dose escalation was taken based on an assessment by investigators of the potential risk of visual toxicities. Visual toxicities at the higher doses (22 mg/m^2 and above) among those tested

Table 3 Summary of PK parameters (mean ± SD, unless otherwise stated) at Cycle 1 Day 1 for blood AUY922 [28–70 mg/m^2 (four highest doses)]

AUY922 PK parameter	AUY922 dose (mg/m^2)			
	28 ($n = 5$)	40 ($n = 3$)	54 ($n = 6$)	70 ($n = 8$)
T_{max} [median, h (range)]	0.50 (0.48–1.07)	1.05 (0.50–1.05)	0.76 (0.48–1.17)	1.02 (0.23–1.17)
C_{max} (ng/ml)	457 ± 101	710 ± 42	1,050 ± 118	1,100 ± 118
$AUC_{(0-last)}$ (h·ng/ml)	6,810 ± 1,090	6,960 ± 1,270	8,880 ± 1,710	8,540 ± 895
$AUC_{(0-inf)}$ (h·ng/ml)	9,550 ± 2,460	11,400 ± 3470[a]	12,300 ± 2720[a]	12,600 ± 1,720
CL (l/h)	4.79 ± 1.68	5.74 ± 1.16[a]	7.24 ± 1.97[a]	8.60 ± 1.30
V_z (l)	646 ± 111	980 ± 132[a]	1,190 ± 151[a]	1,570 ± 293
$T_{1/2}$ (h)	98.7 ± 23.0	123.0 ± 40.8[a]	120.0 ± 28.5[a]	127.0 ± 18.8

PK pharmacokinetics, *SD* standard deviation

[a] Data missing for one patient

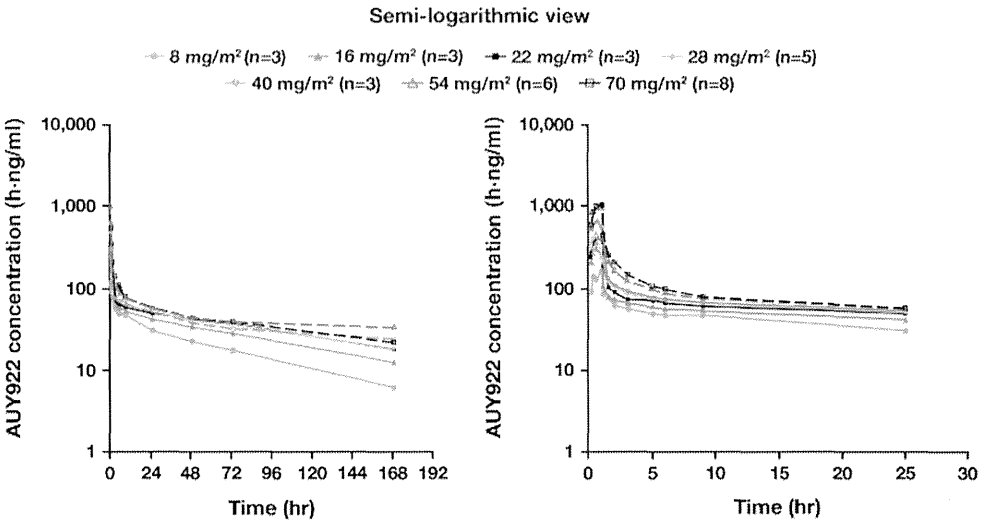

Fig. 1 Mean AUY922 concentration–time profiles in blood on Cycle 1 Day 1

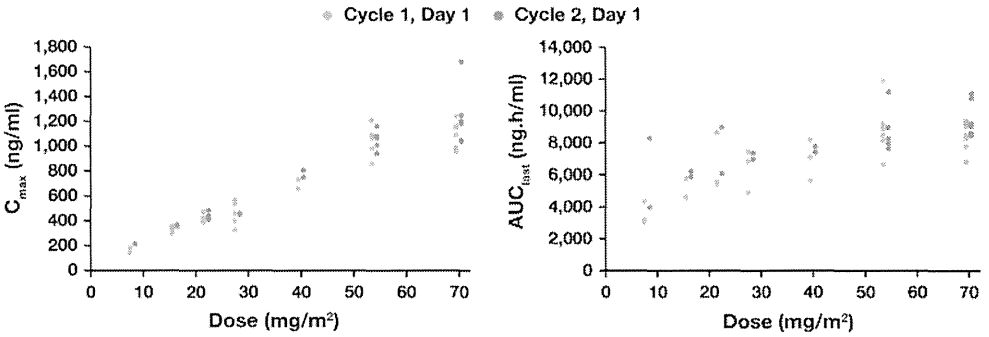

Fig. 2 Relationship between AUY922 dose and blood pharmacokinetics parameters

were observed, most commonly night blindness and photopsia, although these were only Grade 1 or 2. As a result, the MTD was not determined, and the RP2D was, therefore, declared as 70 mg/m^2 once-weekly IV over 1 h.

Pharmacokinetics

AUY922 reached peak concentrations in blood around the end of the infusion. Following the initial rapid decline in concentration levels after the IV administration was completed, blood AUY922 concentration declined slowly, with a mean $T_{1/2}$ of 127 h at 70 mg/m^2 (Table 3; Fig. 1). The $T_{1/2}$ was prolonged with increasing dose (64 h at 8 mg/m^2 to 127 h at 70 mg/m^2). C_{max} for both AUY922 and the metabolite BJP762 generally increased in a dose-proportional manner over the entire dose range. AUC_{last} of AUY922 increased with dose (from 8 to 28 mg/m^2), but was saturated at higher dose levels (Fig. 2; Tables 3, 4). Due to limited sampling time points, the plasma concentration–time profile could not be fully characterized; C_{max} and AUC for AUY922 in plasma had a tendency to increase in a dose-proportional manner even at the higher dose levels (40–70 mg/m^2).

Table 4 Summary of PK parameters (mean ± SD, unless otherwise stated) at Cycle 1 Day 1 for blood BJP762 [28–70 mg/m^2 (four highest doses of AUY922)]

BJP762 PK parameter	AUY922 dose (mg/m^2)			
	28 ($n = 5$)	40 ($n = 3$)	54 ($n = 6$)	70 ($n = 8$)
T_{max} [median, h (range)]	1.07 (1.05–1.17)	1.05 (1.05–1.07)	1.08 (1.02–1.22)	1.13 (1.00–1.23)
C_{max} (ng/ml)	611 ± 201	964 ± 775	1,060 ± 569	1,330 ± 904
$AUC_{(0-last)}$ (h·ng/ml)	3,700 ± 2,170	5,690 ± 5,250	6,320 ± 4,650	5,530 ± 3,320
$AUC_{(0-inf)}$ (h·ng/ml)	3,940 ± 2,320	5,830 ± 5,300	6,770 ± 5200[a]	5,020 ± 3340[b]
$T_{1/2}$ (h)	59.1 ± 28.8	33.1 ± 12.1	49.1 ± 24.0[a]	46.5 ± 27.9[b]

PK pharmacokinetics, *SD* standard deviation

[a] Data missing for one patient

[b] Data missing for two patients

Table 5 Best overall response (Response Evaluation Criteria in Solid Tumors)

Response, *n*	AUY922 dose (mg/m^2)							
	8 ($n = 3$)	16 ($n = 3$)	22 ($n = 3$)	28 ($n = 5$)	40 ($n = 3$)	54 ($n = 6$)	70 ($n = 8$)	Total, *n* (%) ($N = 31$)
Complete response	0	0	0	0	0	0	0	0
Partial response	0	0	0	0	0	1	0	1 (3)
Stable disease	1	1	0	1	1	1	5	10 (32)
Progressive disease	2	2	3	4	2	3	3	19 (61)
Unknown	0	0	0	0	0	1	0	1 (3)
Overall response rate (CR + PR)	0	0	0	0	0	1	0	1 (3)
Disease control rate (CR + PR + SD)	1	1	0	1	1	2	5	11 (36)

Blood PK profiles for AUY922 on Day 1 of Cycle 2 were similar to those on Day 1 of Cycle 1. The geometric mean of accumulation ratios for C_{max} (Day 1 of Cycle 1 to Day 1 of Cycle 2) ranged from 1.01 to 1.28. The ratios for AUC_{last} (Day 1 of Cycle 1 to Day 1 of Cycle 2) ranged between 0.992 and 1.60. Hence, there was no significant drug accumulation with once-weekly IV doses of AUY922.

Efficacy

One patient (rectal carcinoid tumor with lung metastatic lesions) achieved a confirmed partial response (PR) for a duration of >7 months (Table 5; Fig. 3). Ten patients (32 %) achieved a best overall response of stable disease (SD) lasting ≥8 weeks, including five out of the eight patients (63 %) in the 70-mg/m^2 cohort; no patients achieved a complete response. The disease control rate (DCR; PR + SD) across all dose levels was 36 % (Table 5).

Discussion

There are a number of HSP90 inhibitors under clinical development, both as single agents and in combination with other agents [19, 20]. Hepatotoxicity has been reported in both the early and late stages of development of geldanamycin-based HSP90 inhibitors [21, 22]. In this study in Japanese patients with advanced solid tumors, single-agent AUY922 demonstrated an acceptable safety profile at dose levels of 8–70 mg/m^2 with potential clinical activity (DCR 36 %). The MTD was not established, and although the BLRM would have permitted further dose escalation, a decision was made not to escalate the dose any further than the well-tolerated dose of 70 mg/m^2 based on the potential risk of visual toxicity, the symptoms of which were similar to those reported in the preceding global phase I study (CAUY922A2101), and the RP2D was thus declared as 70 mg/m^{2}once-weekly.

Hepatotoxicity was not reported as a frequent AE suspected to be related to study drug, or as a DLT; the most common AEs suspected to be related to this study drug included Grade 1 or 2 diarrhea (65 %), night blindness (42 %) and nausea (23 %). Only Grade 1 or 2 visual AEs (most commonly night blindness and photopsia) were reported at the 22–70 mg/m^2 dose levels. Similar safety findings were observed in the preceding global Phase I CAUY922A2101 study [14]. Visual disturbances have been reported with other geldanamycin and non-geldanamycin

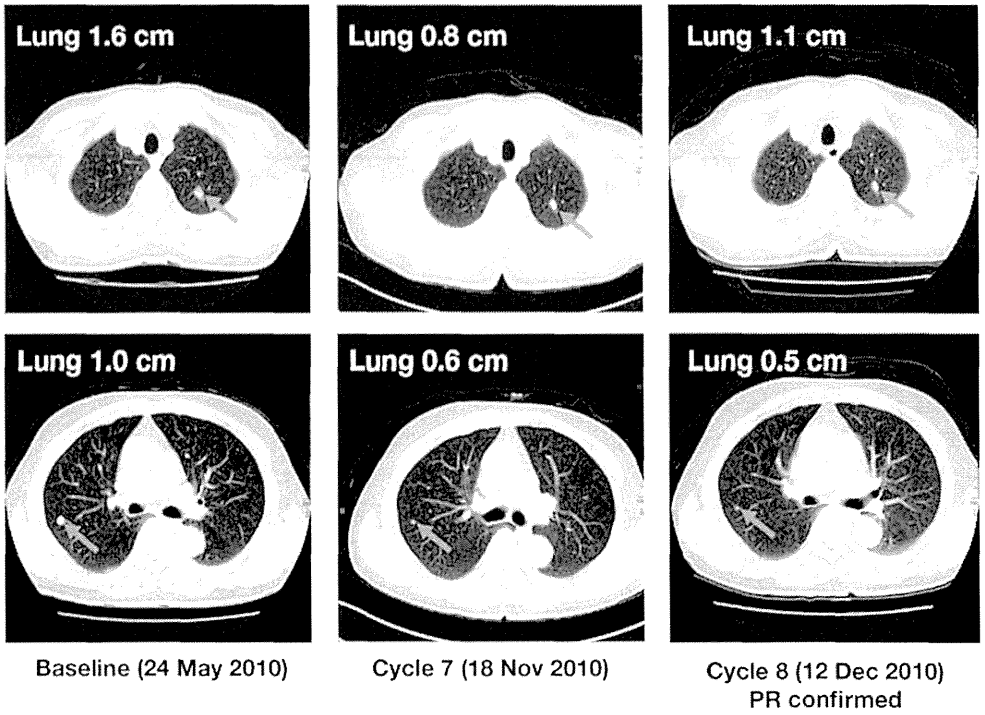

Fig. 3 Computed tomography scans of lung metastases in a patient with a confirmed PR following treatment with AUY922 54 mg/m^2 (63 years old, male, primary rectal carcinoid tumor)

HSP90 inhibitors [23–25]. These visual AEs are regarded as class adverse effects, which are possibly related to tissue distribution of water-soluble agents facilitating a high retina:plasma concentration ratio, as well as the retinal elimination profile [26]. The safety profile of AUY922 was similar to that reported in the preceding CAUY922A2101 study [14], and ongoing Phase II studies [15, 16]. C_{max} for AUY922 in blood increased generally in a dose-proportional manner over the entire dose range. Blood PK parameters of AUY922 in Japanese patients were also comparable to those observed in non-Japanese patients in the CAUY922A2101 study [14]. AUC for AUY922 in blood increased with dose at lower doses, but was saturated at higher doses. This less than dose-proportional increase in blood AUY922 is likely caused by a concentration-dependent and saturable blood cell partition of AUY922. There was no significant drug accumulation following once-weekly intravenous infusion of AUY922.

In summary, AUY922 has shown an acceptable safety profile and demonstrated promising clinical activity in Japanese patients, with one patient achieving a confirmed prolonged PR, and several patients achieving long duration SD at higher dose levels.

Acknowledgments The authors would like to thank the participating patients, their families, all study investigators and research coordinators. Medical editorial assistance was provided by Matthew Naylor, PhD, and was funded by Novartis Pharmaceuticals.

Conflict of interest Toshihiko Doi has received honoraria and research funding from Novartis. Takayuki Yoshino has received honoraria from Takeda, Chugai and Merck Serono, and research funding from Yakult, Taiho, Daiichi-Sankyo, and Lily. Kentaro Yamazaki has received promotional material fees from Takeda and Chugai, and research funding from Taiho and Merck Serono. Narikazu Boku has received honoraria from Taiho, Daiichi-Sankyo, Ono, Yakult, Shionogi, and Takeda, and research funding from Taiho. Matthew Robson and Mikhail Akimov are employees of Novartis, with stock ownership. Other authors have no disclosures to make. This study was designed under the responsibility of Novartis Pharmaceutical Corporation, in conjunction with the steering committee. The study was funded by Novartis Pharmaceuticals Corporation, who collected and analyzed the data and contributed to the interpretation of the study. All authors had full access to all the data in the study, and had final responsibility for the decision to submit for publication.

References

1. Banerji U (2009) Heat shock protein 90 as a drug target: some like it hot. Clin Cancer Res 15:9–14
2. Mahalingam D, Swords R, Carew JS, Nawrocki ST, Bhalla K, Giles FJ (2009) Targeting HSP90 for cancer therapy. Br J Cancer 100:1523–1529
3. Chiosis G, Neckers L (2006) Tumor selectivity of Hsp90 inhibitors: the explanation remains elusive. ACS Chem Biol 1:279–284
4. Neckers L, Workman P (2012) Hsp90 molecular chaperone inhibitors: are we there yet? Clin Cancer Res 18:64–76
5. Pearl LH, Prodromou C, Workman P (2008) The Hsp90 molecular chaperone: an open and shut case for treatment. Biochem J 410:439–453